GDCh Research Article Angewandte International Edition Chemie www.angewandte.org

How to cite: *Angew. Chem. Int. Ed.* **2024**, *63*, e202409527
doi.org/10.1002/anie.202409527

Biochemistry

Pomotrelvir and Nirmatrelvir Binding and Reactivity with SARS-CoV-2 Main Protease: Implications for Resistance Mechanisms from Computations

Johanna Schillings, Carlos A. Ramos-Guzmán, J. Javier Ruiz-Pernía, and Iñaki Tuñón**

Abstract: We investigate the inhibition mechanism between pomotrelvir and the SARS-CoV-2 main protease using molecular mechanics and quantum mechanics/molecular mechanics simulations. Alchemical transformations where each P*i* group of pomotrelvir was transformed into its counterpart in nirmatrelvir were performed to unravel the individual contribution of each group to the binding and reaction processes. We have shown that while a γ-lactam ring is preferred at position P1, a δ-lactam ring is a good alternative for the design of inhibitors for variants presenting mutations at position 166. For the P2 position, tertiary amines are preferred with respect to secondary amines. Flexible side chains at the P2 position can disrupt the preorganization of the active site, favouring the exploration of non-reactive conformations. The substitution of the P2 group of pomotrelvir by that of nirmatrelvir resulted in a compound, named as C2, that presents a better binding free energy and a higher population of reactive conformations in the Michaelis complex. Analysis of the chemical reaction to form the covalent complex has shown a similar reaction mechanism and activation free energies for pomotrelvir, nirmatrelvir and C2. We hope that these findings could be useful to design better inhibitors to fight present and future variants of the SARS-CoV-2 virus.

Introduction

There are two possible strategies to fight COVID-19, the disease caused by SARS-CoV-2 virus: the use of vaccines and antivirals.[1,2] These two strategies are threatened by the variability and continuous adaptation of the virus, which makes continuous research necessary for the improvement of both.[3] Resistance mechanisms to the use of nirmatrelvir, the active principle of Paxlovid, a FDA approved antiviral drug developed by Pfizer, have been already reported.[4] Nirmatrelvir is a covalent inhibitor of the SARS-CoV-2 main protease (M^{pro}), or 3CL protease. This enzyme is a cysteine protease playing an essential role in the replication cycle of the virus, performing most of the cleavage events on the pp1a and pp1ab polyproteins produced post RNA translation. Cleavage of the polyproteins results in the formation of functional non-structural proteins needed by the virus during its replication cycle. One of the advantages of nirmatrelvir is that it can be administered orally, facilitating the treatment of COVID-19 patients. However, certain mutations observed in variants of the M^{pro} increase the virus resistance to treatments with nirmatrelvir by reducing the affinity between the drug and the enzyme and thereby decreasing the efficiency of the treatment.[5–7] This has stimulated the search of new drugs targeting this protease with the aspiration to develop an arsenal of possibilities to fight different variants that may appear with the clinical use of current antivirals.

Pomotrelvir is a covalent inhibitor of the SARS-CoV-2 M^{pro}, recently developed by Pardes Biosciences,[8] presenting the same nitrile warhead as nirmatrelvir (see Figure 1). Once in the active site, these drugs react with the catalytic cysteine (Cys145) forming a thioimidate adduct. The postulated reaction mechanism involves the activation of the catalytic dyad by a proton transfer from Cys145 to His41, forming an ion pair (IP). After this activation, the reaction proceeds through a water-mediated proton transfer from His41 to the nitrogen atom on the nitrile group, concerted with the nucleophilic attack of the Sγ atom of Cys145 to the electrophilic carbon on the nitrile group.[9] Nirmatrelvir and pomotrelvir differ in the substituents appearing after the warhead, denoted as P*i* (see Figures 1a and 1b), which are designed to fit into the corresponding S*i* subsites of the enzymatic active site. In nirmatrelvir the P1 group is a γ-lactam ring, whilst in pomotrelvir it is a δ-lactam ring. The presence of a lactam ring in this position is a common feature in most inhibitors of SARS-CoV and SARS-CoV-2

[*] J. Schillings, C. A. Ramos-Guzmán, J. J. Ruiz-Pernía, I. Tuñón
Departamento de Química Física, Universitat de València, 46100 Burjassot (Spain)
E-mail: carlos.a.ramos@uv.es
ignacio.tunon@uv.es
C. A. Ramos-Guzmán
Instituto de Materiales Avanzados, Universidad Jaume I, 12071 Castelló (Spain)

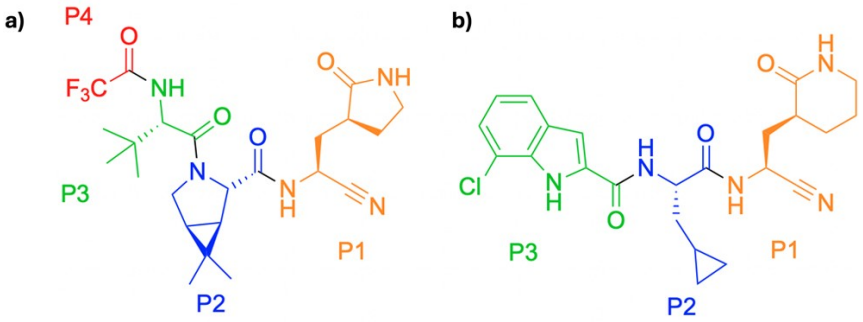

Figure 1. a) P1–P4 groups of nirmatrelvir and b) P1–P3 groups of pomotrelvir.

M^{pro}, exploiting the requirement for a glutamine residue just before the cleavage site in these enzymes.[10] Both drugs present small hydrophobic groups at the P2 position, inspired by the preference shown by this protease for a leucine residue placed in the same position in its natural substrate. A gem-dimethylcyclopropylproline is used in nirmatrelvir, while a cyclopropylmethyl group is found in pomotrelvir. Recent studies show that the nature of the P2 group can have an important impact on the inhibitory potency of nitrile-based compounds.[11] Finally, nirmatrelvir features two chemical groups in its P3 and P4 positions while pomotrelvir has a larger, more conformationally restricted group at its P3 position. In general, the specificity for P3 and P4 positions is lower, although the chemical nature of these groups may affect the stability of the compounds.[9,11,12]

The presence of similarities and differences between these two drugs offer the opportunity to analyse, from a computational point of view, the role of the different P*i* groups during the binding process of the inhibitor (I) into the active site of the enzyme (E) to form the noncovalent enzyme inhibitor complex (EI) and during the reaction that results in the formation of a covalent complex (E–I):

$$E + I \underset{k_{-1}}{\overset{k_1}{\rightleftharpoons}} EI \xrightarrow{k_2} E - I$$

A comparative analysis between these two drugs can reveal the role of the different groups and the advantages/disadvantages of each choice. In this regard, it is interesting to note that, despite the promising results reached by pomotrelvir in the phase 1 of its clinical trials, Pardes Biosciences recently decided to halt its development after the results from its phase 2 trials because the drug was not effective enough in reducing the viral load in patients.[13] This underscores the necessity to conduct further research on the design of new compounds, with the goal of not only improving inhibitory properties towards the wild-type SARS-CoV-2 M^{pro} but also towards potential variants that can compromise the efficiency of current treatments based in nirmatrelvir.

In the present study, we used a combination of Molecular Dynamics (MD) simulations and alchemical transformations with Molecular Mechanics (MM) potentials to analyse the binding pose and relative binding free energies of pomotrelvir and several derivatives, where the impact of different P*i* groups has been evaluated (see Figure S1). We also used hybrid Quantum Mechanics/Molecular Mechanics (QM/MM) free energy calculations to investigate the covalent inhibition process using a multi-dimensional approach (see Figure 2). Computational details are provided in the methodological section in the Supporting Information. Our results focus on the role of the P1 and P2 groups, highlighting some principles that can be used to improve the design of future drug candidates targeting SARS-CoV-2 M^{pro}.

Results and Discussion

Non-Covalent Complex

The Michaelis complex model between the SARS-CoV-2 M^{pro} and pomotrelvir demonstrated high stability across the three replicas of 1 μs. As Figure S2 illustrates, minor fluctuations for the root mean square deviation (RMSD) of the inhibitor and protein atoms can be observed. The P1 group fits into a subpocket, S1, which is formed by residues Phe140, Leu141, Ser144, Glu166, His172, and Ser1 of protomer B (henceforth referred to as Ser1′); the P2 cyclopropylmethyl group establishes non-polar interactions with His41, His164, Met165 and Asp187 while the amino backbone group is hydrogen bonded to Gln189 side chain

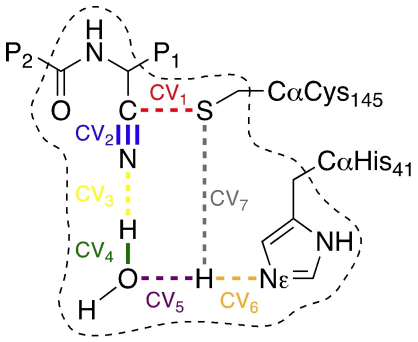

Figure 2. Illustration of the Collective Variables (CVs) and QM region employed to describe the inhibition reaction mechanism of SARS-CoV-2 M^{pro} with pomotrelvir.

(see Figure 3a). The P3 group is largely exposed to the solvent, but it also displays a hydrogen bond interaction to the backbone of Glu166 and a non-polar contact with Met165.

The hydrogen bond pattern established by pomotrelvir in the active site of SARS-CoV-2 M^{pro} can be compared to the one obtained for nirmatrelvir inhibitor with the same enzyme[9] (see Figure 3b). The hydrogen bond patterns are almost identical for both inhibitors, although subtle differences were spotted. One of the differences is a decrease in the strength of interactions observed between the P1 group of pomotrelvir and Glu166 compared to the interactions formed by the P1 group of nirmatrelvir with the same residue. This variation is likely attributed to the bulkier nature of the δ-lactam ring of pomotrelvir compared to the γ-lactam ring of nirmatrelvir. The carboxylate side chain (Cδ atom) group of Glu166 is found at an average distance of 3.65 ± 0.31 Å from the NH group of the γ-lactam ring in nirmatrelvir, while this distance increases to 3.96 ± 0.41 Å in the case of pomotrelvir (see Figure 3c and S3a). This change in the interaction of the P1 group between nirmatrelvir and pomotrelvir could be an advantage for the use of the latter to fight the coronavirus variants presenting the E166V mutation in the M^{pro}. As recently reported, this mutation increases the resistance of the virus to nirmatrelvir.[6] An inhibitor with a δ-lactam substituent at P1 could be a better option to bind to the E166V M^{pro} mutant, because the resulting complex would not be as dependent on the interaction with the side chain of residue 166 as in the case of inhibitors presenting a γ-lactam ring at the same position.

One striking difference between both inhibitors is tied to a key structural variation between the P2 groups in nirmatrelvir and pomotrelvir. The latter presents a cyclopropylmethyl group as side chain in this position, while the mainchain amino group is a secondary amine that can act as a hydrogen bond donor with the carbonyl oxygen atom of Gln189. Instead, nirmatrelvir includes a gem-dimethylcyclopropylproline group at P2, transforming the mainchain amino group into a tertiary amine unable to act as hydrogen bond donor. This structural change between the inhibitors results in a weaker interaction of the P2 group of nirmatrelvir with Gln189 compared to pomotrelvir, as observed in Figure 3b and Figure S3b. It must be noticed, as discussed below, that this additional protein-inhibitor hydrogen bond interaction does not necessarily translate into an improved binding energy because one also must consider the interaction of the inhibitor with the solvent.

Finally, the P3 group of pomotrelvir is a rigid 7-chloroindole-2-carbonyl group, while in nirmatrelvir there are two groups: *tert*-leucine, P3, and trifluoroacetyl, P4. The two inhibitors establish a similar interaction pattern with Glu166 backbone atoms as show in Figure 3c and Figure 3d, being the interaction slightly tighter in the case of pomotrelvir (see Figure S3c and S3d), which could be related to the reduced flexibility of its P3 group.

The structural differences between both inhibitors also have consequences on the preorganization of the active site. In the left panel of Figure 4a, the distributions of distances between the proton donor and acceptor atoms in the catalytic dyad, Cys145 and His41, are shown in the presence of inhibitor pomotrelvir or nirmatrelvir, respectively. As said before, the proton transfer from cysteine to histidine is the first step that activates the enzyme for covalent inhibition. It can be observed that the catalytic dyad is more

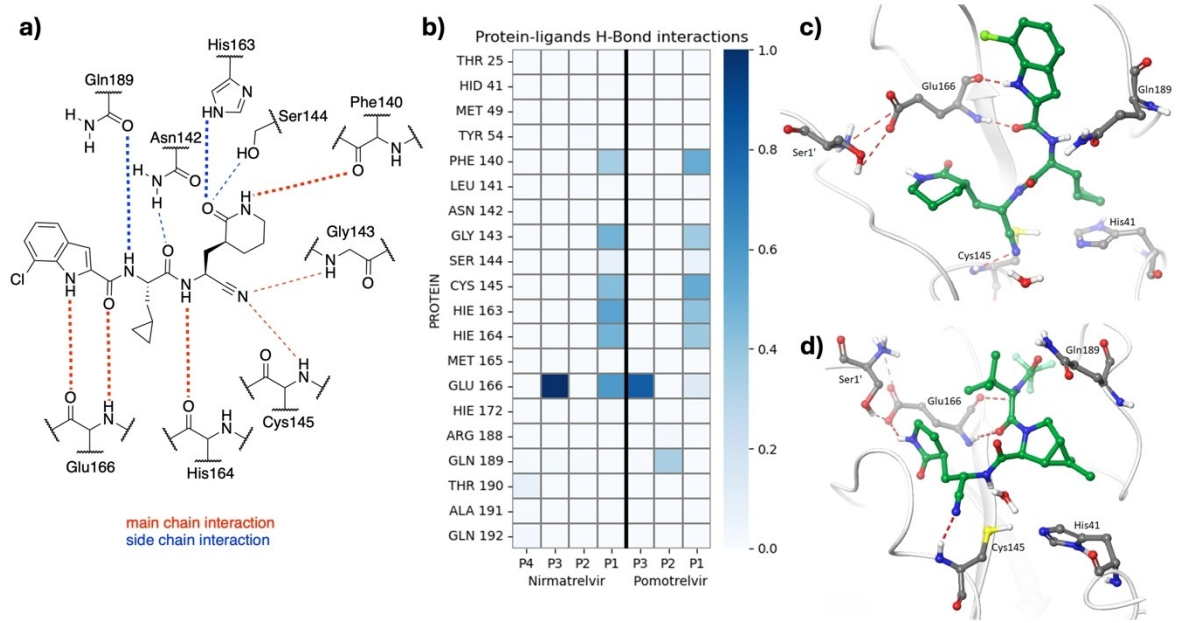

Figure 3. Michaelis Complex formed between pomotrelvir and nirmatrelvir with the SARS-CoV-2 M^{pro}. a) Schematic representation of the hydrogen bonds between pomotrelvir and the M^{pro}. b) Frequency of protein-inhibitor hydrogen bond interactions. The colour intensity corresponds to the observed frequency between inhibitors Pi groups and residues of the M^{pro} during MD simulations. c) Binding pose of pomotrelvir. d) Binding pose of nirmatrelvir.

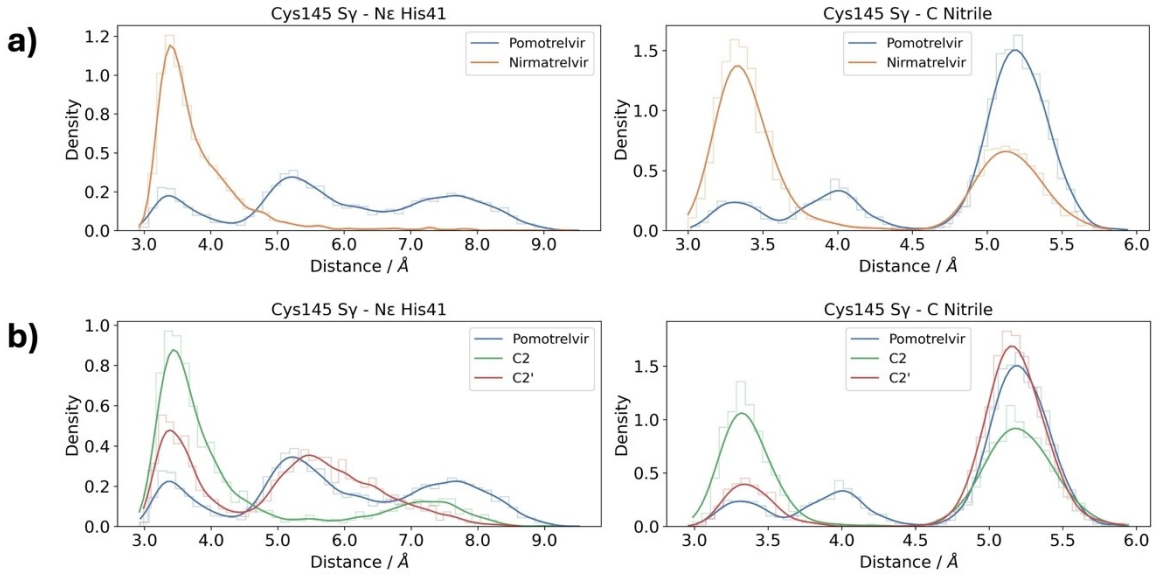

Figure 4. Effect of the cyclization of P2 in the reactive populations in the Michaelis complex. Distribution function of the Cys145 Sγ atom relative to the His41 Nε atom (left) and to the carbon atom in the nitrile group (right). In presence of the inhibitors a) pomotrelvir and nirmatrelvir, b) pomotrelvir C2 and C2′, respectively.

frequently positioned for a direct proton transfer from Cys145 to His41 with nirmatrelvir, orange curve, than with pomotrelvir, blue curve. Likewise, the right panel of Figure 4b indicates a closer positioning of Cys145 with respect to the inhibitor warhead to perform the nucleophilic attack in nirmatrelvir than in pomotrelvir.

These differences can be attributed to the behaviour of the P2 side chain group of pomotrelvir. Figure S4 illustrates how this group is flexible in the active site and when it rotates around the Cα–Cβ bond induces a conformational change in the surroundings. Figure S4 shows the disruption of the hydrogen bond interaction between the mainchain nitrogen atom in Gln189 and the oxygen atom in Met49 occurring after the pomotrelvir P2 group rotation. Breaking the Gln189–Met49 hydrogen bond leads to a separation of the regions defined by residues Ile43 to Leu67 in domain I and Val186 to Ala191 in domain II (see Figure S5) opening the active site and increasing the distance between the catalytic dyad. Our MD simulations show that even upon the return of the P2 side chain group to its initial position, both hydrogen bond interactions struggle to be re-established. Thus, the binding of pomotrelvir could alter the preorganization of the active site needed for the covalent reaction between the inhibitor and the enzyme, decreasing then its inhibitory efficiency.

Alchemical Transformations

Observing the differences in the binding modes of pomotrelvir and nirmatrelvir on the active site of the SARS-CoV-2 M^{pro}, we investigated the impact of P*i* groups on the relative binding free energy contributions of both inhibitors, as an attempt to discern which design could lead to a better affinity with the enzyme. To achieve this, alchemical transformations were performed to create a series of chimeric structures, named C1, C2 and C3, where each of the P*i* groups of pomotrelvir was substituted by the equivalent group in nirmatrelvir. In addition, because of the central role of the P2 group, we also considered the substitution of this group in pomotrelvir by the P2 group from UAWJ9-36-1, a compound with potent binding and enzymatic inhibition against SARS-CoV-2 M^{pro},[14] and named the resulting structure as C2′. Introduction of the P2 group of this compound in nirmatrelvir reduced the IC50 by a factor of 2.3.[14] All alchemical transformations and their associated changes in the relative binding free energies are shown in Figure 5. The averaged values for each transformation in water and in the enzyme are given in Table 1, while the values obtained for each of the five replicas are given in the Table S1.

When the P1 side chain group of pomotrelvir was substituted with the P1 side chain group of nirmatrelvir, there was a small change of -0.9 ± 0.6 kcal·mol^{-1} in the binding free energy, in agreement with the observation

Table 1: Free energy changes for alchemical transformations of pomotrelvir into C1, C2, C3, and C2′ (see Figure 5) in aqueous and protein environments, along with $\Delta\Delta G_{binding}$ values. Estimated free energy values (kcal·mol^{-1}) are the result of five replicas and were obtained using Thermodynamic Integration (see Table S1). The errors correspond to the standard deviations of the mean value.

modification	ΔG_{water}	$\Delta G_{Protein}$	$\Delta\Delta G_{binding}$
C1	-0.1 ± 0.2	-1.0 ± 0.5	-0.9 ± 0.6
C2	12.4 ± 0.2	9.9 ± 0.6	-2.5 ± 0.6
C2′	11.2 ± 0.1	9.7 ± 0.6	-1.5 ± 0.6
C3	-36.7 ± 0.2	-33.7 ± 1.4	3.0 ± 1.4

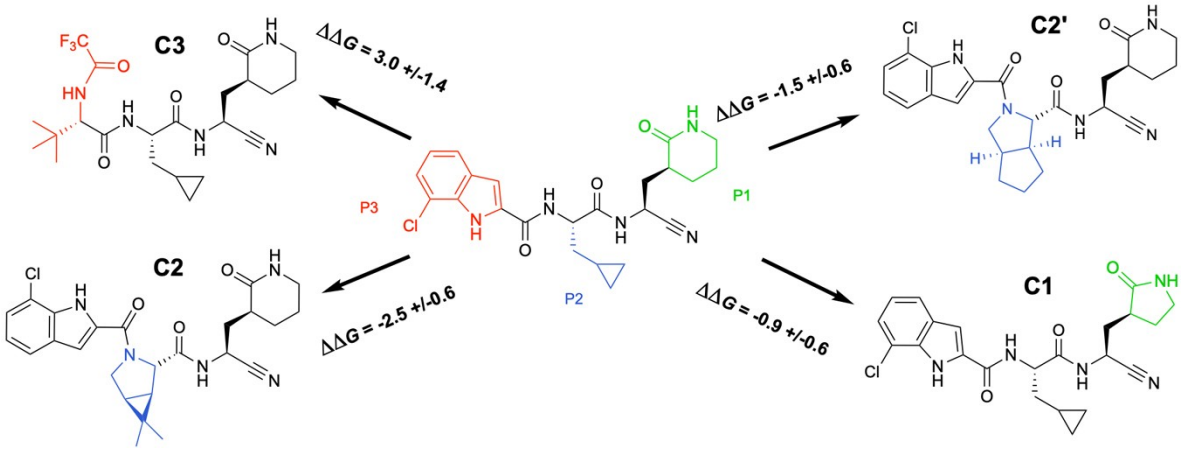

Figure 5. Binding free energies changes related to the transformation of pomotrelvir Pi groups to the Pi groups in nirmatrelvir (C1 to C3) and the P2 group in UAWJ9-36-1, C2′. The error bars correspond to the standard deviation of the mean as determined from five independent simulations (see Table S1).

made before that the NH group of nirmatrelvir γ-lactam ring interacts better with Glu166 than the δ-lactam ring of pomotrelvir. In any case the difference observed is small and close to the statistical error. Overall, these results indicate that a γ-lactam ring could be a reasonable alternative to the δ-lactam ring at position P1.

More significant changes in the binding free energy were observed upon modification of the P2 group of pomotrelvir. A destabilizing effect was observed during the transformation to C2 and C2′ both in water and in the enzyme, see Table 1. The presence of a secondary amine in the pomotrelvir P2 group allows for hydrogen bonding interactions with water molecules in the solvent and with the Gln189 Oγ atom once the Michaelis complex (MC) is formed, as shown in Figure S6. In contrast, these interactions are not present in the case of the tertiary amine in the P2 group of nirmatrelvir (C2) or in the P2 group of UAWJ9-36-1 (C2′), as reflected in the distribution of Gln189 Cδ–N P2 distances, see Figure S6b. This structural analysis is complemented by the decomposition of the P2 group-protein interaction energies carried out for the three inhibitors (see Figure S7 and Table S2). This decomposition shows that the larger difference among them is found in the more favourable electrostatic interaction of the P2 group with Gln189 in the case of pomotrelvir. For the P2 group, changes in the van der Waals interactions are relatively less important, although the P2 groups of C2 and C2′ present slightly improved van der Waals interactions to Met49 and Met165, respectively. In water, a solvation shell of ~2 water molecules is observed for pomotrelvir up to 3.5 Å of the amino group, while for C2 and C2′ only one water molecule is solvating its tertiary amino group around 4 Å. For pomotrelvir in the enzyme, a weaker hydrogen bond is established with the Gln189 Oγ atom, as shown in Figure S6. Thus, the presence of a secondary amine disfavours the process of transferring the inhibitor from the solvent to the active site. The overall transformation of pomotrelvir into C2 or C2′ results in a notable improvement in binding energy, with an associated decrease of -2.5 ± 0.6 kcal·mol^{-1} and -1.5 ± 0.6 kcal·mol^{-1}, respectively. This transformation of the secondary amine group in pomotrelvir to a tertiary amine group in C2 and C2′, unable to act as proton donor, seems to be the key to the overall binding energy improvement. Missing this hydrogen bond interaction destabilizes more the inhibitor in water than in the active site, leading to a better relative binding free energy.

Apart from the effects associated to the main chain transformation, we have previously shown that the presence of a flexible side chain in the P2 group of pomotrelvir induces the opening of the M^{pro} active site, due to the disruption of the hydrogen bond between Gln189 and Met49. When the P2 group of pomotrelvir is changed by a cyclized version, as in C2 or C2′, we observe a noticeable increase of the fraction of conformations where this hydrogen bond is preserved (see Table S3). According to these results, obtained from three independent 1 μs simulations of the Michaelis complexes formed with pomotrelvir, C2 and C2′, the Gln180-Met49 hydrogen bond is present in approximately 24 % of configurations with pomotrelvir, while for the chimeric structures C2 and C2′, this percentage is increased to 54 % and 42 %, respectively—values comparable to those observed for nirmatrelvir. We also monitored the hydrogen bond length between the catalytic dyad (Cys145–His41) and the distance from the nucleophilic Sγ atom of Cys145 to the electrophilic carbon atom of the nitrile warheads, see Figure 4b. The complexes formed with C2 and C2′ display more frequently short distances compatible with the requirements of the chemical reaction leading to the formation of the covalent complex between the inhibitor and the enzyme. This analysis supports the hypothesis that the presence of a flexible P2 side chain in pomotrelvir favours the loss of preorganization of the active site, disfavouring then the formation of the covalent complex.

Remarkably, the substitution of the rigid 7-chloroindole-2-carbonyl group at the P3 position of pomotrelvir with the *tert*-leucine and trifluoroacetyl groups in nirmatrelvir resulted in a destabilising effect on the relative binding free

energy (see Table 1). This effect might be attributed to the presence of three fluorine atoms, one secondary amine group and two carbonyls in C3 that facilitate stronger interactions with both the solvent and the enzyme, unlike the P3 group of pomotrelvir, which only has one secondary amine group and one carbonyl group in this region to form hydrogen bonds. Note also that the larger flexibility of P3/P4 groups in nirmatrelvir can impose an entropic penalty to the binding process due to a restriction of their conformational freedom in the active site.

Formation of the Covalent Complex

Our investigation of the multidimensional free energy surface for the chemical reaction between SARS-CoV-2 M^{pro} and pomotrelvir, using the adaptive string method (ASM),[15] reveals a minimal free energy path (MFEP) similar to that previously reported for nirmatrelvir.[9] The resultant free energy profile and the progression of the CVs throughout the reaction path are depicted in Figures 6a and 6b, respectively, while the one corresponding to nirmatrelvir, at the same computational level, is shown in Figure S8. According to the evolution of the Collective Variables (CVs), see Figure 6b, the process starts with the activation of the catalytic dyad, with the proton transfer from Cys145 to His41 (see the evolution of the Sγ-Hγ and Hγ-Nε distances), followed by the intervention of a water molecule that works as a proton shuttle between His41 and the nitrile inhibitor group (see the change in the Hw-Ow, N-Hw, Hγ-Nε and Ow-Hγ distances) and the nucleophilic attack of Cys145 Sγ atom on the electrophilic carbon atom of the nitrile warhead (see the evolution of the Sγ-C distance in Figure 6b).

A first energy barrier of 6.2 ± 0.2 kcal·mol^{-1} was identified. This barrier is associated with the proton transfer from the catalytic Cys145 to His41, to form the catalytic dyad in the ion pair (IP1) configuration. Figure 6b shows that during the transfer of the proton from Cys145 Sγ to His41 Nε the oxygen atom of the water molecule comes closer to the Hγ atom, reducing the distance from 4.18 Å in the reactant state to 3.14 Å in the IP1 state. This contributes to stabilize the IP1, which presents a relative free energy with respect to the reactants of 4.7 ± 0.2 kcal·mol^{-1}. The geometry of IP1 is shown in Figure 6c. IP1 rearranges into a higher-energy configuration IP2 (shown in Figure 6d) with a free energy of 6.6 ± 0.5 kcal·mol^{-1}. The observed increase in energy is associated to the separation of the catalytic dyad in such a way that the activated Cys145 comes closer to the electrophilic carbon atom of the inhibitor (the Sγ-C diminishes to 2.12 Å). This process is assisted by the formation of the hydrogen bond between the water molecule and the nitrogen atom in the nitrile group (N-Hw), and between the Hγ atom (now bonded to His41) and the oxygen atom of the

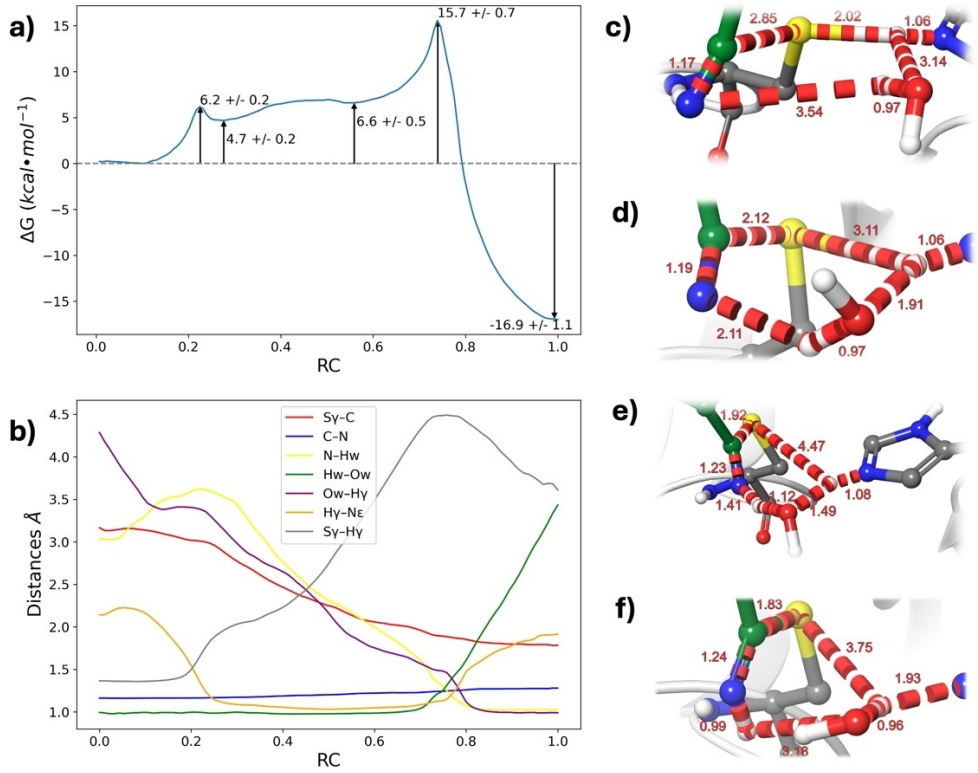

Figure 6. Formation of the E–I complex between pomotrelvir and SARS-CoV-2 M^{pro}. a) B3LYPD3/6-31+G*/MM free energy profile along the path-CV. b) Evolution of the CVs (in Å) along the MFEP. The definition of the CVs is found in Figure 2. c) IP1 structure, d) IP2 structure, e) TS and f) product. The error bars correspond to the standard deviation of the mean as obtained from bootstrapping error analysis (see methodology section).

water molecule (Ow-Hγ). At this point the distance of the triple C-N bond has been slightly lengthened from 1.17 Å in the reactant state to 1.19 Å.

From IP2, the reaction reaches the rate-determining Transition State (TS), with an activation free energy of 15.7 ± 0.7 kcal·mol^{-1}, a value similar to the value derived from the experimental rate constant for the reaction of the M^{pro} with a peptidic substrate (18.2 kcal·mol^{-1})[16] and to the value determined at the same computational level for nirmatrelvir (16.3 kcal·mol^{-1}).[9] This activation energy for the covalent inhibition process is also similar to the value derived from the experimental rate constants obtained for a hydroxymethyl ketone inhibitor (18.8 kcal·mol^{-1}).[17] At this TS the nucleophilic attack is almost completed, with the Sγ-C distance decreasing to 1.92 Å. This stage is characterized by the exchange of two protons: one proton moves from His41 to the water molecule, while the other one moves from the water to the nitrogen atom in the nitrile group of the inhibitor, as seen in Figure 6e. Significantly, the water molecule acting as a proton shuttle is taking over the role played by the leaving amino group when the reaction takes place with its natural substrate,[18] see Figure S9. The process culminates in the final product state where the water-assisted proton transfer is complete. This results in the formation of an exergonic thioimidate product (-16.9 ± 1.1 kcal·mol^{-1}), characterized by an Sγ-C distance of 1.83 Å, as shown in Figure 6f.

An additional confirmation of the adequacy of the description obtained from the B3LYPD3/MM simulations is provided by the M06-2X/MM complementary simulations, presented in Figure S10. The formation of the covalent complex with pomotrelvir at the M06-2X/MM level is almost structurally identical to that described here. Also, the free energy profile is very similar, with an activation free energy of 17.9 kcal·mol^{-1} at the M06-2X level (to be compared to the 15.7 kcal·mol^{-1} barrier obtained at the B3LYPD3 level). The reaction free energies are also in good agreement, -18.6 versus -16.9 kcal·mol^{-1}, respectively.

From the alchemical transformation study, it was observed that the chimeric structure C2 had better binding energies. This makes it a strong candidate for studying the formation of the covalent E–I complex using the same methodology applied to pomotrelvir. As expected, the mechanism obtained for C2 is very similar to the one observed for pomotrelvir and nirmatrelvir (see Figure S11). No major changes are observed in the evolution of the CVs during the chemical reaction with C2 when compared to pomotrelvir. The formation of the ion pair structure in the presence of C2 is favoured with respect to pomotrelvir, with a free energy cost of only 2.3 ± 0.1 kcal·mol^{-1}, close to the value reported for nirmatrelvir.[9] For C2, the activation free energy barrier obtained for the formation of the covalent complex is 16.1 ± 0.6 kcal·mol^{-1}, very similar to the value computed for pomotrelvir. While the reaction with pomotrelvir is slightly more exergonic than with C2, -16.9 ± 1.1 and -13.5 ± 1.2 kcal·mol^{-1} respectively, both values are clearly more negative than the value obtained for the reaction with nirmatrelvir, -9.5 kcal·mol^{-1}.[9] In this way, the reversibility of the inhibition with C2 does not seem to be a matter of concern. In summary, the change of the cyclopropylmethyl group of pomotrelvir to the gem-dimethylcyclopropylproline present in C2 has some advantages as it improves the binding free energy of the inhibitor, stabilizes the IP structure while the exergonicity of the reaction to form the covalent E–I product is not compromised.

As discussed earlier, we observed a larger conformational flexibility of the active site in the MC of the enzyme with pomotrelvir compared to nirmatrelvir. The high mobility is attributed to the non-cyclic nature of the P2 side chain present in pomotrelvir. Interestingly, this effect is reversed in C2, where the P2 group of pomotrelvir was replaced by the P2 group of nirmatrelvir. The comparison of the distribution of distances between the Cys145 Sγ and the His41 Nε atoms in the MC formed with pomotrelvir and C2 shows an increase in the population of reactive configurations in the latter (see Figure S12), in concordance with the larger population of configurations where the hydrogen bond between residues Gln189 and Met49 is present (Table S3). The increase in the population of the reactive structures represents an additional advantage for the inclusion of cyclic P2 groups in the designing process of inhibitors for this enzyme. We can estimate the effect on the activation free energy by fitting the probability distributions, presented in Figure S12, to a combination of gaussian distribution functions, each one corresponding to a different conformation (see Table S4 for details). For pomotrelvir, the free energy cost required to exist in a reactive conformation (with a short Cys145–His41 hydrogen bond length) is of about 1.1 kcal·mol^{-1}, whereas only 0.15 kcal·mol^{-1} is needed for C2. This effect on the preorganization of the active site supports the use of other groups different to cyclopropylmethyl at the P2 position of nitrile inhibitors.

Conclusions

Using a combination of pure MM and hybrid QM/MM methodologies, the covalent inhibition of the SARS-CoV-2 M^{pro} by pomotrelvir has been studied. We first analysed the formation of the noncovalent complex and as well as the contribution of each of its P*i* fragments to the relative binding free energy of the inhibitors. We then determined the reaction mechanism for the formation of the covalent enzyme-inhibitor complex. This information can be helpful to formulate strategies to develop more potent inhibitors to fight COVID-19 infection.

Observations obtained from MD simulations suggest that the binding mode of pomotrelvir differs slightly from that of nirmatrelvir. The decrease in the frequency of the hydrogen bond interaction between the P1 group of pomotrelvir and Glu166 could negatively affect the stability of the P1 group in the S1 pocket of the wild type M^{pro}. A γ-lactam ring, present at the P1 position of nirmatrelvir, appears to be a better choice to occupy the P1 position instead of the δ-lactam ring of pomotrelvir, as the former establishes stronger interactions with Glu166, although alchemical transformations point to a small effect on the

relative binding free energy. Nevertheless, this difference in the interaction pattern established by the δ-lactam and γ-lactam rings could turn into a potential advantage for the inhibition of the E166V variant of the M^{pro}.

Regarding the P2 group, the substitution of the cyclopropylmethyl moiety in pomotrelvir by a gem-dimethylcyclopropylproline group, as in nirmatrelvir, increases the binding free energy of the inhibitor because the former establishes stronger hydrogen bond interactions in the solvent than in the enzyme through its secondary amine. The cyclisation of the side chain also favours the formation of reactive conformations leading to the covalent complex. Consequently, the gem-dimethylcyclopropylproline group is considered as a more suitable choice to occupy the P2 position than the cyclopropylmethyl group present in pomotrelvir.

Regarding the P3 group of pomotrelvir, the substitution of the 7-chloroindole-2-carbonyl group with *tert*-leucine and trifluoroacetyl groups, as those found at positions P3 and P4 of nirmatrelvir, decrease the binding free energy of the inhibitor. Both P3 groups of pomotrelvir and nirmatrelvir establish robust interactions with Glu166 side chain. As commented before, the description of these interactions can be of interest for the design of new inhibitors, particularly if mutations in residue 166 are anticipated as a resistance mechanism of the virus against the treatments with nirmatrelvir.

As expected, the reaction mechanism obtained from our simulations for the formation of the covalent complex between the M^{pro} and pomotrelvir is very similar to that described for nirmatrelvir. The catalytic Cys145 must be activated by a proton transfer to His41 that leads to the formation of an ion pair, followed by a shuttle proton transfer mechanism through a water molecule from His41 to the nitrogen atom of the nitrile warhead and the nucleophilic attack of the Cys145 Sγ atom to the electrophilic carbon atom of the warhead. The activation free energy associated with the covalent inhibition is 15.7 $kcal \cdot mol^{-1}$. As discussed above, the kinetics of the process could be favoured by replacing the cyclopropylmethyl group of pomotrelvir with the gem-dimethylcyclopropylproline of nirmatrelvir. The MC formed with the resulting inhibitor, C2, disturbs less the active site, facilitating the exploration of reactive conformations, while the activation free energy as determined from these conformations is almost identical (16.1 $kcal \cdot mol^{-1}$). From the thermodynamic perspective, the exergonicity is decreased by 3.4 $kcal \cdot mol^{-1}$ when the enzyme reacts with C2 with respect to pomotrelvir, but it is still 4.0 $kcal \cdot mol^{-1}$ more exergonic than for the covalent inhibition with nirmatrelvir.

As a summary, the combination of simulations performed in this work shows some important findings that can be useful to assist in the design of new inhibitors of SARS-CoV-2 M^{pro}, particularly for the selection of the groups in P1 and P2 positions. We have shown that a δ-lactam ring is an adequate choice to be incorporated at the P1 position in the design of inhibitors designed against M^{pro}, especially those variants presenting mutations at position 166. For the P2 position, tertiary amines are clearly preferred with respect to secondary amines. The possibility to act as a hydrogen bond donor seem to favour more the interaction with the solvent than with the protein, decreasing the affinity for the enzyme. In addition, flexible groups at the P2 position disfavour the formation of the covalent complex because they can disrupt the preorganization of the active site, favouring the dynamical exploration of non-reactive conformations. Regarding the reaction mechanism to form the covalent enzyme-inhibitor complex, all the inhibitors analysed here, pomotrelvir, nirmatrelvir and C2, present a very similar mechanism and activation free energy, according to our simulations. We hope that all these findings could be useful to fight present and future variants of SARS-CoV-2 virus, especially considering that the efficacy of nirmatrelvir for nonhospitalized patients is questioned.[19]

Acknowledgements

The authors thank financial support from grant PID2021-123332OB-C22 funded by MCIN/AEI/10.13039/501100011033/ and by "ERDF A way of making Europe" and from grant PROMETEO CIPROM/2021/079 of Generalitat Valenciana. We want to acknowledge Barcelona Supercomputing Center (BSC) for providing us access to MareNostrum and the staff from BSC for the technical support.

Conflict of Interest

The authors declare no conflict of interest.

Data Availability Statement

The data that support the findings of this study are available in the supplementary material of this article.

Keywords: SARS-COV-2 main protease · pomotrelvir · nirmatrelvir · QM/MM · free energy

[1] B. Bolon, W. M. Haschek, *Toxicol. Pathol.* **2020**, *48*, 718–720.
[2] D. R. Owen, C. M. N. Allerton, A. S. Anderson, L. Aschenbrenner, M. Avery, S. Berritt, B. Boras, R. D. Cardin, A. Carlo, K. J. Coffman, A. Dantonio, L. Di, H. Eng, R. Ferre, K. S. Gajiwala, S. A. Gibson, S. E. Greasley, B. L. Hurst, E. P. Kadar, A. S. Kalgutkar, J. C. Lee, J. Lee, W. Liu, S. W. Mason, S. Noell, J. J. Novak, R. S. Obach, K. Ogilvie, N. C. Patel, M. Pettersson, D. K. Rai, M. R. Reese, M. F. Sammons, J. G. Sathish, R. S. P. Singh, C. M. Steppan, A. E. Stewart, J. B. Tuttle, L. Updyke, P. R. Verhoest, L. Wei, Q. Yang, Y. Zhu, *Science* **2021**, *374*, 1586–1593.
[3] J. Zhang, T. Xiao, Y. Cai, C. L. Lavine, H. Peng, H. Zhu, K. Anand, P. Tong, A. Gautam, M. L. Mayer, R. M. Walsh, S. Rits-Volloch, D. R. Wesemann, W. Yang, M. S. Seaman, J. Lu, B. Chen, *Science* **2021**, *374*, 1353–1360.
[4] D. Jochmans, C. Liu, K. Donckers, A. Stoycheva, S. Boland, S. K. Stevens, C. De Vita, B. Vanmechelen, P. Maes, B. Trüeb, N. Ebert, V. Thiel, S. De Jonghe, L. Vangeel, D. Bardiot, A.

Jekle, L. M. Blatt, L. Beigelman, J. A. Symons, P. Raboisson, P. Chaltin, A. Marchand, J. Neyts, J. Deval, K. Vandyck, *mBio* **2023**, *14*, e02815–22.
[5] C. A. Ramos-Guzmán, M. Andjelkovic, K. Zinovjev, J. J. Ruiz-Pernía, I. Tuñón, *Chem. Sci.* **2023**, *14*, 2686–2697.
[6] N. S. Zuckerman, E. Bucris, D. Keidar-Friedman, M. Amsalem, T. Brosh-Nissimov, *Clin. Infect. Dis.* **2023**, ciad494.
[7] H. T. H. Chan, A. S. F. Oliveira, C. J. Schofield, A. J. Mulholland, F. Duarte, *JACS Au* **2023**, *3*, 1767–1774.
[8] X. Tong, W. Keung, L. D. Arnold, L. J. Stevens, A. J. Pruijssers, S. Kook, U. Lopatin, M. Denison, A. D. Kwong, *Antimicrob. Agents Chemother.* **2023**, *67*, e00840–23.
[9] C. A. Ramos-Guzmán, J. J. Ruiz-Pernía, I. Tuñón, *Chem. Commun.* **2021**, *57*, 9096–9099.
[10] R. Hilgenfeld, *FEBS J.* **2014**, *281*, 4085–4096.
[11] M. Zhu, T. Fu, M. You, J. Cao, H. Yang, X. Chen, Q. Zhang, Y. Xu, X. Jiang, L. Zhang, H. Su, Y. Zhang, J. Shen, *Bioorg. Med. Chem.* **2023**, *87*, 117316.
[12] S. T. Ngo, T. H. Nguyen, N. T. Tung, B. K. Mai, *RSC Adv.* **2022**, *12*, 3729–3737.
[13] Pardes Biosciences, Inc., "PBI-0451 (Pomotrelvir) Phase 2 Study in Nonhospitalized Symptomatic Adults With COVID-19," can be found under https://clinicaltrials.gov/study/NCT05543707 **2023**.
[14] Z. Xia, M. Sacco, Y. Hu, C. Ma, X. Meng, F. Zhang, T. Szeto, Y. Xiang, Y. Chen, J. Wang, *ACS Pharmacol. Transl. Sci.* **2021**, *4*, 1408–1421.
[15] K. Zinovjev, I. Tuñón, *J. Phys. Chem. A* **2017**, *121*, 9764–9772.
[16] S. Ullrich, K. B. Ekanayake, G. Otting, C. Nitsche, *Bioorg. Med. Chem. Lett.* **2022**, *62*, 128629.
[17] M. Yu Zakharova, A. A. Kuznetsova, V. I. Uvarova, A. D. Fomina, L. I. Kozlovskaya, E. N. Kaliberda, I. N. Kurbatskaia, I. V. Smirnov, A. A. Bulygin, V. D. Knorre, O. S. Fedorova, A. Varnek, D. I. Osolodkin, A. A. Ishmukhametov, A. M. Egorov, A. G. Gabibov, N. A. Kuznetsov, *Front. Pharmacol.* **2021**, *12*, 773198.
[18] C. A. Ramos-Guzmán, J. J. Ruiz-Pernía, I. Tuñón, *ACS Catal.* **2020**, *10*, 12544–12554.
[19] J. Hammond, R. J. Fountaine, C. Yunis, D. Fleishaker, M. Almas, W. Bao, W. Wisemandle, M. L. Baniecki, V. M. Hendrick, V. Kalfov, J. A. Simón-Campos, R. Pypstra, J. M. Rusnak, *N. Engl. J. Med.* **2024**, *390*, 1186–1195.

Manuscript received: May 25, 2024
Accepted manuscript online: July 3, 2024
Version of record online: September 2, 2024